JOURNAL OF GUIDANCE, CONTROL, AND DYNAMICS
Vol. 21, No. 3, May–June 1998

Robust, Decoupled, Flight Control Design with Rate-Saturating Actuators

S. A. Snell* and R. A. Hess†
University of California, Davis, Davis, California 95616

Techniques for the design of control systems for manually controlled, high-performance aircraft must provide the following: 1) multi-input/multi-output solutions, 2) acceptable handling qualities including no tendencies for pilot-induced oscillations, 3) performance and stability robustness in the presence of significant plant uncertainty, 4) minimum performance degradation in the presence of actuator saturation (particularly rate saturation), and 5) a tractable approach for compensator design. A design technique built upon quantitative feedback theory is offered as a candidate methodology that can provide flight control systems meeting these requirements and that does so over a considerable part of the flight envelope. An example utilizing a simplified model of a supermaneuverable fighter aircraft demonstrates the proposed design methodology.

Nomenclature

$\boldsymbol{A}, \boldsymbol{B}, \boldsymbol{C}, \boldsymbol{D}, \boldsymbol{E}, \boldsymbol{F}$	= matrices used in the state-space description of the vehicle and dynamic inverse precompensation
E_p	= $p_c - p$, deg/s
E_β	= $\beta_c - \beta$, deg
F_β, F_p	= quantitative feedback theory (QFT) prefilters
$\boldsymbol{G}_c(\boldsymbol{s})$	= diagonal QFT compensation matrix
$\boldsymbol{G}_{c_p}(\boldsymbol{s})$	= nondiagonal dynamic inverse precompensation matrix
$G_r(s)$	= washed-out yaw-rate feedback element
$\boldsymbol{K}$	= control distribution matrix
$L(s)$	= loop transmission
$\boldsymbol{P}(\boldsymbol{s})$	= plant matrix
$\boldsymbol{P}_e(\boldsymbol{s})$	= effective plant matrix including dynamic inverse precompensator $\boldsymbol{G}_{c_p}(\boldsymbol{s})$
$p(t)$	= vehicle body-axis roll rate, deg/s
$p_c(t)$	= roll-rate command, deg/s
$r(t)$	= vehicle body-axis yaw rate, deg/s
$\boldsymbol{u}(\boldsymbol{t})$	= vector output of dynamic inverse compensator $\boldsymbol{G}_{c_p}(\boldsymbol{s})$
$\boldsymbol{v}(\boldsymbol{t})$	= vector input in dynamic inverse state-space system
$\boldsymbol{w}_i(\boldsymbol{t})$	= vector of pseudoinputs and vector output of QFT compensation matrix $\boldsymbol{G}_c(\boldsymbol{s})$
$\boldsymbol{y}(\boldsymbol{t})$	= vector of system outputs in state-space description of vehicle
$\beta(t)$	= vehicle sideslip angle, deg
$\delta_A(t)$	= aileron deflection, deg
$\delta_{\mathrm{DT}}(t)$	= differential horizontal stabilizer deflection, deg
$\delta_R(t)$	= rudder deflection, deg
$\delta_{\mathrm{RTV}}(t)$	= differential pitch thrust vectoring, deg
$\delta_{\mathrm{YTV}}(t)$	= yaw thrust vectoring, deg

Introduction

THE flight control system design technique to be described is an outgrowth of several recent research efforts.[1–5] The work has been motivated by the realization that a significant number of high-performance aircraft, particularly those with fly-by-wire flight control systems, have experienced shortcomings in control and handling qualities in developmental flight tests.[6] These problems, some of which have been quite severe, can often be attributable to a failure of the control system design technique to provide 1) acceptable handling qualities including no tendencies for pilot-induced oscillations, 2) performance and stability robustness in the presence of significant plant uncertainty, and 3) minimum performance degradation in the presence actuator saturation (particularly rate saturation). Of course, any flight control system design technique should also provide 4) multi-input/multi-output (MIMO) solutions and 5) a tractable approach for compensator design.

In the following, a methodology is presented for meeting the requirements just stated. For the sake of clarity, the methodology will be couched in terms of a specific flight control example. The example presents a challenging problem, and the vehicle model is readily available for the interested reader. A description of the example problem begins the presentation. This is followed by a discussion of the quantitative feedback theory (QFT) procedure, with particular emphasis upon the direct determination of an approximately diagonalizing precompensator that makes the MIMO QFT design easier, and the use of a predesign technique (PDT) that offers considerable insight into the formal QFT design. A procedure for lessening performance degradations in the presence of actuator rate saturation follows. The results of the QFT design are then presented including a nonlinear simulation in which actuator amplitude and rate saturation are considered. A statement of conclusions closes the discussion.

Flight Control Example

System Structure

Figure 1 is a block diagram representation of the flight control design to be discussed: the determination of a stability and command augmentation system for the lateral-directional control of a high-performance aircraft. The vehicle in question is represented by a simplified model of a supermaneuverable fighter aircraft whose linearized dynamics are given in Ref. 7, and that, in one form or another, has been used in a variety of related studies.[2,8,9] There are 15 flight conditions to be considered in the design, ranging from Mach number of 0.3 and altitude of 10,000 ft, to Mach number of 0.9 and altitude of 30,000 ft.

Starting from the far right in Fig. 1, the lateral-directional dynamics of the vehicle are presented by the matrix of plant transfer functions $\boldsymbol{P}(\boldsymbol{s})$. The vehicle response variables to be controlled are body-axis roll rate $p(t)$ and sideslip angle $\beta(t)$. An inner feedback loop involving feedback of washed-out yaw rate $r(t)$ is employed to improve Dutch-roll damping across the 15 flight conditions. As shown in Fig. 1, the vehicle possesses five lateral-directional control effectors: differential horizontal tail δ_{DT}, aileron δ_A, rudder δ_R, differential pitch thrust vectoring δ_{RTV}, and yaw thrust vectoring δ_{YTV}. The matrix $\boldsymbol{K}$ is a 5×2 control distribution matrix, each row of which contains only a single nonzero entry. For reasons discussed in Ref. 2, this nonzero entry is set equal to the rate limit (degrees per second) of the particular (and only) control surface actuator that

Received June 2, 1997; revision received Jan. 2, 1998; accepted for publication Jan. 9, 1998.

*Assistant Professor, Department of Mechanical and Aeronautical Engineering. Senior Member AIAA.

†Professor, Department of Mechanical and Aeronautical Engineering. Associate Fellow AIAA.

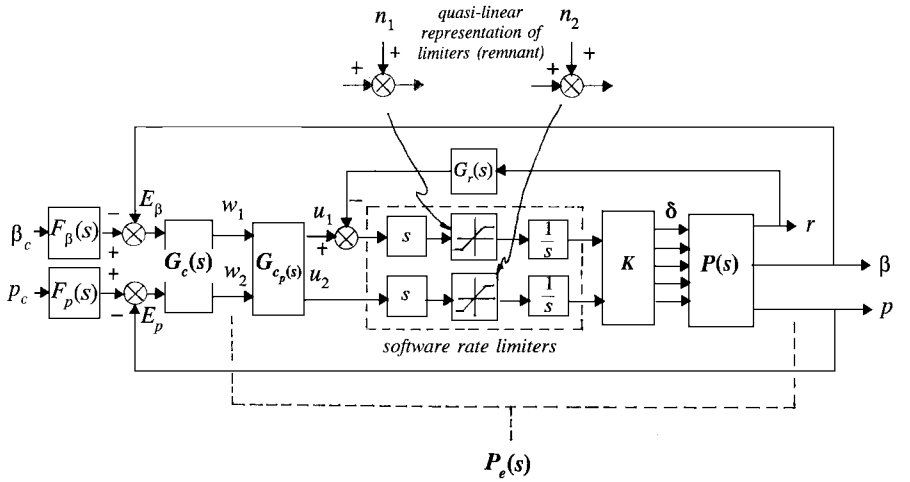

Fig. 1 Flight control system structure.

it effects. Selection of the control effectors to associate with each output variable was made on the basis of the control effectiveness of each device.

The control distribution matrix allows the use of software rate limiters, each of which is defined by three elements (differentiator, limiter, and integrator) providing inputs to $\boldsymbol{K}$. It is important to point out that the differentiators s in Fig. 1 are always subsumed into the compensators that precede them, e.g., the elements of the matrix compensator $\boldsymbol{G}_{c_p}(s)$ and the single element $G_r(s)$. This is generally easy to accomplish because these elements typically contain integrators. If this is not the case, then an additional high-frequency pole must be added to ensure properness.

Performance and Stability Specifications

The control system performance specifications are stated as performance and stability bounds. The performance bounds relate to the magnitudes of the following transfer functions evident in Fig. 1: $|(\beta/\beta_c)(j\omega)|$, $|(p/p_c)(j\omega)|$, $|(\beta/p_c)(j\omega)|$, and $|(p/\beta_c)(j\omega)|$. The first two of these functions define tracking bounds, whereas the latter two define cross-coupling bounds. For the tracking bounds, both upper and lower limits are prescribed, whereas for the cross-coupling bounds, only upper limits are needed. In addition to the performance bounds just described, stability bounds are also defined. These may be handled in a number of ways, but here will be specified as maximum amplitude ratios on the closed-loop transfer functions defining tracking behavior.

In this example, attention will be focused on roll attitude as the variable of interest to the pilot in manual, closed-loop tracking. Sideslip will not be considered as a tracking variable, although specifications will still be placed on input–output and cross-coupling relations as just described. In Ref. 3, a pilot modeling procedure is described that allows the prediction of handling qualities using what is termed a handling qualities sensitivity function (HQSF). By examining the flight test results from 32 different vehicle/control configurations and modeling the corresponding pilot/vehicle systems, frequency-domain bounds were determined for the HQSF corresponding to level 1 and level 2 handling qualities. In addition, frequency-domain bounds for the power spectral density of a feedback signal in the pilot/vehicle model were determined related to pilot-induced oscillation (PIO) susceptibility. These techniques will be used here to prescribe the roll-rate tracking bounds $|(p/p_c)(j\omega)|$ so as to yield predicted level 1 handling qualities (assuming a roll-attitude loop is closed by the pilot) and no predicted susceptibility to PIOs across the 15 flight conditions.

QFT Procedure

Introduction

The application of QFT to flight control problems has been described rather extensively in the literature, e.g., Ref. 10. No detailed discussion of the QFT design philosophy will be presented. Two issues that can present difficulties in MIMO QFT designs will, however, be addressed. First, QFT can be difficult to apply successfully when there is significant cross coupling between control loops. Second, it is difficult to know a priori what performance objectives may be reasonably obtained, particularly as regards control cross coupling. These problems are addressed by using a diagonalizing precompensator to decouple aircraft outputs, whereas a PDT helps in indicating what performance may be achievable in the formal QFT design. The PDT is undertaken with a reduced-order plant and simplified compensator structure, to be discussed.

Diagonal Compensation

As typically applied, the QFT design procedure involves input–output pairing. This means associating one or more control effectors exclusively with the control of an output or response variable. With this accomplished, one is left with a diagonal compensation matrix, and the so-called method 1 (original) or method 2 (improved) QFT design techniques are followed.[11] Either of these approaches places the burden of providing desired tracking and cross-coupling performance on the elements of the diagonal compensation matrix. It is obvious that some reduction in conservatism can be gained by a design procedure that employs a nondiagonal compensation matrix. A number of such approaches have been suggested for achieving nondiagonal compensation,[12–14] all of which create a precompensation matrix [shown in Fig. 1 as $\boldsymbol{G}_{c_p}(\boldsymbol{s})$]. For the QFT design, this precompensation matrix is considered part of the plant matrix [now referred to as the effective plant matrix $\boldsymbol{P}_e(\boldsymbol{s}) = \boldsymbol{P}(\boldsymbol{s})\boldsymbol{G}_{c_p}(\boldsymbol{s})$] and a diagonal QFT compensation matrix is then designed [shown in Fig. 1 as $\boldsymbol{G}_c(\boldsymbol{s})$]. The diagonal $\boldsymbol{G}_c(\boldsymbol{s})$ and nondiagonal $\boldsymbol{G}_{c_p}(\boldsymbol{s})$ are combined to yield the final compensator $\boldsymbol{G}_{c_p}(\boldsymbol{s}) \cdot \boldsymbol{G}_c(\boldsymbol{s})$ to be implemented in the flight control computer.

A problem that can occur with previous methods for achieving nondiagonal compensation is that it may be quite difficult to design the diagonal QFT compensator given the effective plant formed by the original plant and the precompensation matrix. This is because, although the effective plant $\boldsymbol{P}_e(\boldsymbol{s})$ may be nearly diagonal, it may exhibit poor gain-phase properties, which make it difficult to compensate with the QFT procedure. This problem can be overcome by the procedure outlined next.

Precompensation Using Dynamic Inversion

Dynamic inversion is a well-known technique for designing decoupling controllers for nonlinear systems using static, full-state feedback.[15,16] An extension of dynamic inversion using dynamic compensation with partial-state feedback will be applied to the linearized aircraft model to produce a precompensator $\boldsymbol{G}_{c_p}(\boldsymbol{s})$ that approximately decouples the roll and sideslip responses. Dynamic inversion is an excellent candidate for forming a precompensation matrix for QFT because the designer is able to specify the dynamics of a $\boldsymbol{P}_e(\boldsymbol{s})$ that is amenable to relatively simple compensation using the Nichols chart, the primary graphical tool for QFT design. This is achieved as follows. Consider the square, linear, time-invariant

system, with an $n \times 1$ state vector $\boldsymbol{x}(t)$, an $m \times 1$ input vector $\boldsymbol{u}(t)$, and an $r \times 1$ output vector $\boldsymbol{y}(t)$:

$$\dot{\boldsymbol{x}} = \boldsymbol{A}\boldsymbol{x} + \boldsymbol{B}\boldsymbol{u} \tag{1a}$$

$$\boldsymbol{y} = \boldsymbol{C}\boldsymbol{x} + \boldsymbol{D}\boldsymbol{u} \tag{1b}$$

The output variables [elements of $\boldsymbol{y}(t)$] are β and p and the input variables [elements of $\boldsymbol{u}(t)$] are the ganged control effector commands shown in Fig. 1. The $\boldsymbol{D}$ matrix in Eq. (1b) is zero. A decoupling control law can be obtained by differentiating the individual elements of $\boldsymbol{y}(t)$ a sufficient number of times until a term involving an element of the input $\boldsymbol{u}(t)$ appears. The second-order actuator dynamics of the five control effectors must be appended to the basic rigid-body aircraft dynamics resulting in a plant with 14 states. In this case, three differentiations of both β and p are required before $\boldsymbol{u}(t)$ appears. The output equation then becomes

$$\boldsymbol{y}^{[3]} = \boldsymbol{F}\boldsymbol{x} + \boldsymbol{E}\boldsymbol{u} \tag{2}$$

where $\boldsymbol{F} = \boldsymbol{C}\boldsymbol{A}^3$ and $\boldsymbol{E} = \boldsymbol{C}\boldsymbol{A}^2\boldsymbol{B}$. A sufficient condition for the existence of a decoupling control is that $\boldsymbol{E}$ in Eq. (2) has full rank r. If this is the case, the decoupling control law is given by the dynamic system

$$\dot{\boldsymbol{x}}_G = [\boldsymbol{A} - \boldsymbol{B}\boldsymbol{E}^{-1}\boldsymbol{F}]\boldsymbol{x} + \boldsymbol{B}\boldsymbol{E}^{-1}\boldsymbol{v} \tag{3a}$$

$$\boldsymbol{u} = -\boldsymbol{E}^{-1}\boldsymbol{F}\boldsymbol{x} + \boldsymbol{E}^{-1}\boldsymbol{v} \tag{3b}$$

where $\boldsymbol{E}^{-1}$ is a right pseudoinverse of $\boldsymbol{E}$ and where the new input $\boldsymbol{v}$ is related directly to the output through Eqs. (2) and (3a) to give

$$\boldsymbol{v} = \boldsymbol{y}^{[3]} \tag{4}$$

The dynamics now appear as three pure integrators in each channel. Desirable linear dynamics between each output y_i and new external inputs w_i are given by setting

$$v_i = -a_{i0}y_i - a_{i1}\dot{y}_i - a_{i2}\ddot{y}_i + b_i w_i \tag{5}$$

This sets the transfer function between w_i and y_i to be

$$\frac{y_i}{w_i}(s) = \frac{b_i}{s^3 + a_{i2}s^2 + a_{i1}s + a_{i0}} \tag{6}$$

In this way, six poles of $\boldsymbol{G}_{c_p}(\boldsymbol{s})$ are placed. This leaves a total of eight other poles to be placed. It is shown in Ref. 16 that the remaining poles are located at the open-loop transmission zeros of the system given by Eq. (1), whereas the original poles of the system in Eq. (1) are canceled exactly by transmission zeros in $\boldsymbol{G}_{c_p}(\boldsymbol{s})$. Clearly, it is essential that the system given by Eq. (1) be stable and minimum phase. Techniques for handling unstable and nonminimum phase systems are discussed in Ref. 16 and include the formation of regulated variables, which are minimum phase.

It is possible to schedule $\boldsymbol{G}_{c_p}(\boldsymbol{s})$ as a function of flight condition so that the decoupling would be nearly exact. This was not done, however, because scheduling a 14-state controller is a nontrivial task and the robustness may be questionable. Instead, a single dynamic inverse was found for the entire set of flight conditions. One way to select this inverse is to consider the entire set of precompensation matrices $\boldsymbol{G}_{c_p}(\boldsymbol{s})$ for all of the flight conditions and then to design a single $\boldsymbol{G}_{c_p}(\boldsymbol{s})$ matrix, one element at a time. For example, the (i, j) element is given by plotting the set of all (i, j) elements on the complex plane and then finding a single transfer function that minimizes the deviation between itself and all other elements. This minimization is carried out over a specific frequency range of interest. In practice, this procedure is usually unnecessary as the $\boldsymbol{G}_{c_p}(\boldsymbol{s})$ associated with one of the configurations being analyzed can usually be selected that approximately meets the criterion just described. Here, the flight condition corresponding to a Mach number of 0.6 and an altitude of 20,000 ft was selected to determine $\boldsymbol{G}_{c_p}(\boldsymbol{s})$.

The effectiveness of using a single dynamic inverse to decouple the plant approximately and to provide simplified effective dynamics for eventual compensation in the formal QFT procedure can often be expedited by the feedback of one or more independent, internal variables prior to calculating any dynamic inverse. Independent internal variables refer to variables other than the response or output variables (or their derivatives). In applications such as flight control, the feedback of internal variables can increase the damping of oscillatory modes and, as such, can improve the ability of a single dynamic inverse to effectively decouple the plant across the range of configurations being considered in the design. This is because the inversion no longer relies on exact cancellation of lightly damped poles and zeros. In the current example, washed-out yaw rate is an internal variable, and using it as a feedback variable proves very effective.

QFT PDT

QFT requires quantitative specification of desired performance and uncertainty. As described in the preceding text, employing QFT in the frequency domain requires the designer to specify bounds on the amplitude ratios of on-axis and off-axis response-to-command transfer functions (desired tracking performance and desired cross-coupling minimization). Whereas specifying tracking bounds is fairly straightforward, especially in flight control problems where handling qualities specifications can provide some guidance, the specification of cross-coupling bounds can be problematic. This is not a minor concern as these cross-coupling bounds can drive the entire QFT design. Finally, MIMO QFT designs are usually approached using a sequential-loop closure technique to minimize conservatism.[11] Until now, no method other than trial and error could be employed to determine the appropriate loop closure sequence. As will be seen, both the problem of determining cross-coupling bounds and loop closure sequence can be solved using an approximate PDT. The details of this technique can be found elsewhere[5]; however, a brief discussion is in order.

The PDT is based on an assumption regarding the diagonal compensation elements of $\boldsymbol{G}_c(\boldsymbol{s})$. Referring to the example, if the pseudo-controls w_1 and w_2 are approximately decoupled, then the following relationships can be employed:

$$G_{c_{\beta\beta}} \approx \frac{\omega_{c_\beta}}{s} \cdot \frac{1}{P_{e11}(s)}, \qquad G_{c_{pp}} \approx \frac{\omega_{c_p}}{s} \cdot \frac{1}{P_{e22}(s)} \tag{7}$$

where the double subscripts on the left-hand sides of the equations represent diagonal elements, $\omega_{c_{()}}$ represent crossover frequencies, and $P_{e11}(s) = \beta/w_1$ and $P_{e22}(s) = p/w_2$. No actuator dynamics are included in determining $\boldsymbol{P}_e(\boldsymbol{s})$ for the PDT design, although, of course, they are included in the formal QFT design discussion later. Equation (7) exploits the well-known fact that the loop transmission $L(s)$ of a well-designed single-input/single-output (SISO) system, or the loop transmissions of an approximately decoupled MIMO system, each resemble $\omega_{c_{()}}/s$ near the region of crossover. Equation (7) extends this approximation to all frequencies. In terms of approximating the elements of $\boldsymbol{G}_c(\boldsymbol{s})$, low-frequency characteristics ($\omega \ll \omega_c$) are relatively unimportant provided $|L(j\omega)| \gg 1.0$, and high-frequency characteristics ($\omega \gg \omega_c$) are relatively unimportant provided $|L(j\omega)| \ll 1.0$. These conditions are guaranteed by Eq. (7). Note that stability is assumed in the PDT. For QFT designs, a nominal plant is selected to define a nominal loop transmission on the Nichols chart. For the PDT, this simply means choosing one of the possible plants out of the uncertain set to define the denominator of the right-hand sides of Eq. (7). With the approximations of Eq. (7), approximate closed-loop transfer functions $(\boldsymbol{I} + \boldsymbol{P}_e\boldsymbol{G}_c)^{-1}\boldsymbol{P}_e\boldsymbol{G}_c F$ can be obtained. Thus, the PDT will yield estimates of tracking and cross-coupling performance, as well as crossover frequencies. These computations can be done very quickly on a personal computer, using readily available computer-aided design software.

Improving Performance in the Presence of Actuator Rate Saturation

It has been demonstrated for a class of control systems that the use of software rate limiters can offer significant improvement in command-following performance when control actuators undergo rate saturation.[2] A pair of such software limiters is shown in Fig. 1. In Ref. 2, the use of such limiters was restricted to a class of systems in which each actuator could receive its input from only one compensated error signal. As demonstrated in Ref. 2, the software

limiters improve performance by ensuring that each actuator never receives an input rate exceeding the limits of the device. In addition, the software limiters come out of saturation as soon as their input rates become smaller than the limiting values. This behavior is in contrast to that of a typical actuator undergoing rate saturation, where the device remains in saturation until the actuator output (a displacement) equals its commanded input. This latter behavior introduces an effective time delay in the control system, often with dire consequences.[6,17] An analytical approach to describing the action of the software limiters can be made by again considering Fig. 1, where now the software limiters have been replaced by injected remnant signals $n_i(t)$. It is assumed that the limiters prevent rate saturation of the actuators themselves, so that the software limiters are the only nonlinearities present in the system. Conceptually, each and every signal in the quasilinear system can be forced to be identical to that in the nonlinear system for any command inputs by the injection of appropriate $n_i(t)$ (where the possibility of amplitude saturation is not considered). Now if one could select elements of the compensator matrix $\boldsymbol{G}_{c_p}(s)$ such that these $n_i(t)$ have no effect on the vehicle response variables, then system performance would be completely unaffected by the presence of the software rate limiters. This would occur because the software limiters are, by design, preventing saturation of the actuators, and the saturation that is occurring in the software devices (represented by the injected remnant) is having no effect on system response. Of course, such a situation is not possible. The effect of the injected remnant can be reduced considerably, however, in a frequency range below crossover. This is accomplished in a loop-shaping design by appropriately selecting the type of the elements in $\boldsymbol{G}_c(s)$, where type refers to the exponent on any free s in the compensator transfer function.

In the work of Ref. 2, for a flight control system similar to that of Fig. 1, explicit expressions were developed for transfer functions $(E_\beta/n_1)(s)$, $(E_\beta/n_2)(s)$, $(E_p/n_1)(s)$, and $(E_p/n_2)(s)$. These expressions were used to develop specifications on the type of the compensators and loop transmissions. These analytical results were predicated on the aforementioned assumption of each actuator being driven by the output of one and only one compensated error signal. By considering $|(\beta/n_1)(j\omega)|$, $|(\beta/n_2)(j\omega)|$, $|(p/n_1)(j\omega)|$, and $|(p/n_2)(j\omega)|$, however, and adjusting the type of the compensator elements to achieve a desired reduction in these magnitudes over a limited but important frequency range (below crossover), the assumption just stated can be obviated. That is, each actuator can be driven by more than one compensated error signal, and the benefits of the software limiters can still be obtained. This is obviously a desirable result from the standpoint of flight control system design wherein control effectors often play multiple roles. As discussed in Ref. 2, a tradeoff exists in this approach, because increasing the type of the compensation elements improves tracking under actuator rate saturation, but reduces linear stability margins. It should be emphasized that, as compared to flight control systems without software limiters, significant performance improvements can be obtained under saturation with the use of these limiters, but stability cannot be guaranteed.

Design

Handling Qualities

The procedure commences by selecting candidate upper and lower tracking bounds for $|(p/p_c)(j\omega)|$. These are then evaluated by constructing the HQSF as discussed in Ref. 3. If the results are unacceptable, then new tracking bounds are selected in an iterative manner. In the pilot/vehicle analysis, each of these bounds are considered to describe the plant of a SISO system under manual control. Figure 2 shows the structural model of the human pilot, which is used to make predictions about handling qualities level and PIO susceptibility. The HQSF is defined as $|(1/K_e)\cdot(U_M/C)(j\omega)|$, where K_e represents a pilot gain and U_M and C are, respectively, proprioceptive feedback and input signals in the structural pilot model of Fig. 2. The structural model parameters are selected as described in Ref. 3. Figure 3 shows the areas outlined by dashed curves, which, if penetrated by the HQSF, predict the handling qualities level indicated in that area. Also shown in the figure are the HQSFs generated by the structural model for the upper and lower p-loop tracking bounds that were selected and used for the remainder of the design.

Boundaries associated with $\Phi_{u_m u_m}(\omega)$, the power spectral density of the signal U_M in the pilot model of Fig. 2, can also be utilized in a manner similar to those for the HQSF. $\Phi_{u_m u_m}(\omega)$ is calculated with a specific input power spectral density.[3] Predicted PIO ratings (PIOR) are determined by the area penetrated by $\Phi_{u_m u_m}(\omega)$ when the structural model parameters are selected as described in Ref. 3. Obviously, tracking bounds selected in this manner are not unique. They are, however, predicted to yield level 1 (satisfactory) handling qualities and a $1 \leq \text{PIOR} \leq 2$ (no tendency for pilot to induce undesirable motions).

As part of the formal QFT design, a limit can be placed on the maximum amplitude peak of any closed-loop transfer function in the tracking loops for the 15 flight conditions considered. By making this limit small, the variations in magnitude of any of the closed-loop tracking transfer functions will not differ significantly in form from those described by the upper and lower bounds. Thus, the

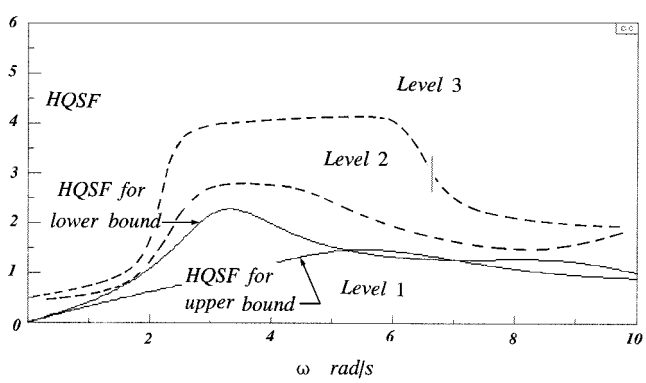

Fig. 3 Handling qualities boundaries for HQSFs.

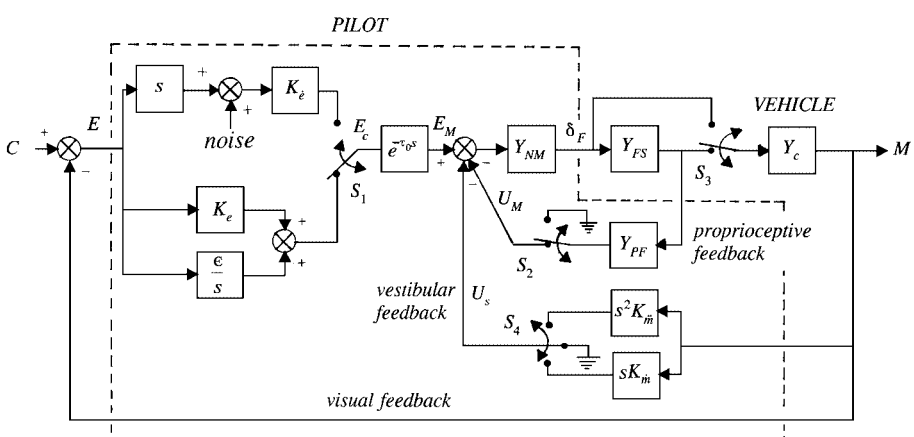

Fig. 2 Structural model of the human pilot.

Table 1 Actuation and control distribution characteristics

Control distribution matrix $\boldsymbol{K}$

$$\boldsymbol{K} = \begin{bmatrix} 0 & 0 & 100 & 0 & 60 \\ 60 & 100 & 0 & 60 & 0 \end{bmatrix}^T$$

Actuator dynamics: $\dfrac{K(z_1)}{(p_1)[\zeta_1, \omega_1]} = \dfrac{K(s+z_1)}{(s+p_1)\left[s^2 + 2\zeta_1\omega_1 s + \omega_1^2\right]}$

δ_{DT}:	$\dfrac{30^2}{[0.707, 30]}$	rate limit = 60 deg/s, amplitude limit = ±17.5 deg
δ_A:	$\dfrac{75^2}{[0.59, 75]}$	rate limit = 100 deg/s, amplitude limit = ±27.5 deg
δ_R:	$\dfrac{72^2}{[0.69, 72]}$	rate limit = 100 deg/s, amplitude limit = ±30.0 deg
δ_{RTV}/δ_{TV}:	$\dfrac{20^2}{[0.6, 20]}$	rate limit = 60 deg/s, amplitude limit = ±30.0 deg

handling qualities and PIO predictions for the bounds will also suffice for any of the flight conditions defining the uncertain plant.

Dynamic Inversion for the PDT

As mentioned in the preceding text, the feedback of yaw rate as an internal variable improved the Dutch-roll damping, making the dynamic inversion less sensitive to changes in flight condition. The feedback transfer function G_r in Fig. 1 was defined as

$$G_r = -3s/(s+1) \tag{8a}$$

or

$$sG_r = \frac{-3s^2}{(s+1)(0.01s+1)} \tag{8b}$$

where Eq. (8b) was used when the software rate limiters were employed, and the differentiating s in Fig. 1 was subsumed into $G_r(s)$ as described earlier. The output of $G_r(s)$ was fed back to the rudder and the yaw-thrust vectoring through the control distribution matrix $\boldsymbol{K}$, shown in Table 1. The washout was employed to allow the pilot to perform coordinated turns.

Because actuator dynamics were neglected in the PDT, the dynamic inversion was applied to the four-state system composed of the rigid-body model at the nominal flight condition plus the simpler washout of Eqs. (8a). The technique led to a nominal effective plant matrix

$$\boldsymbol{P}_e(\boldsymbol{s}) = \begin{bmatrix} 1/s & 0 \\ 0 & 1/s \end{bmatrix} \tag{9}$$

PDT

The PDT allowed the creation of bounds on $|(\beta/\beta_c)(j\omega)|$, $|(p/p_c)(j\omega)|$, $|(\beta/p_c)(j\omega)|$, and $|(p/\beta_c)(j\omega)|$. Figure 4 shows the $|(p/p_c)(j\omega)|$ and $|(p/\beta_c)(j\omega)|$, as well as the predicted performance based on the PDT. The bounds on the roll-rate tracking were selected as described earlier. As also mentioned, bounds on $|(\beta/\beta_c)(j\omega)|$ (not shown) were not based on handling qualities or PIO susceptibility, as the β loop was not considered a tracking loop, per se. The bounds were considered to provide acceptable open-loop response to cockpit pedal inputs. In generating the performance results shown by Fig. 4, the nominal flight condition was chosen with a Mach number of 0.6 and an altitude of 20,000 ft. The loop crossover frequencies defined for the nominal plant were $\omega_{c_\beta} = 3.0$ and $\omega_{c_p} = 6.0$ rad/s. Prefilter transfer functions $F_\beta(s)$ and $F_p(s)$ were also obtained from the PDT design.

Given the tracking bounds and least upper bounds for cross coupling, the formal QFT procedure could begin. In addition to the bounds, estimates of the required QFT compensation, valid in a broad frequency range around the crossover frequencies, could be obtained from Eq. (7).

Dynamic Inversion for the Formal QFT Design

The formal QFT procedure includes models of the actuators that drive the five control effectors. These models, along with the associated rate and amplitude limits, are given in Table 1. The addition of the actuators requires the full-order dynamic inversion design. The dynamics were selected via Eqs. (5) and (6) to yield

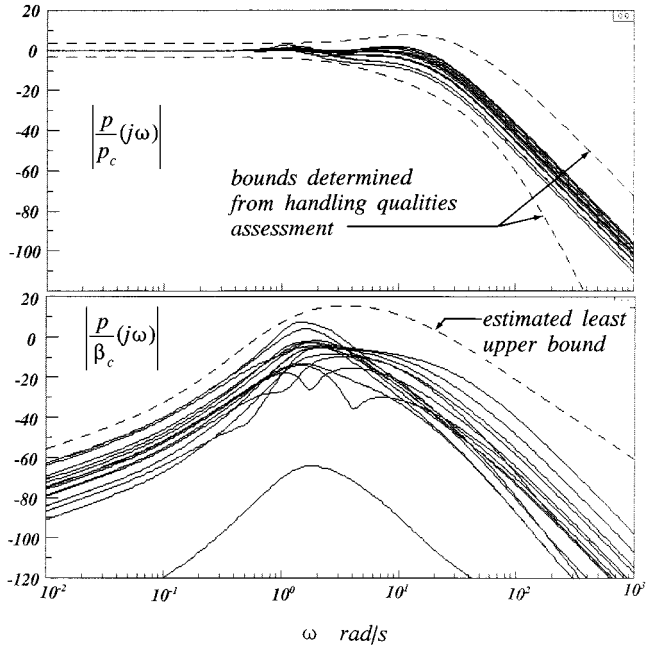

Fig. 4 Performance from the PDT for 15 flight conditions.

$$\boldsymbol{P}_e(\boldsymbol{s}) = \begin{bmatrix} \dfrac{900}{s(s+30)^2} & 0 \\ 0 & \dfrac{900}{s(s+30)^2} \end{bmatrix} \tag{10}$$

As mentioned, six poles of the effective plant $\boldsymbol{P}_e(\boldsymbol{s})$ can be placed with the design, but the plant plus actuators and yaw-rate feedback now has 14 states. The pair of poles in each diagonal element of the effective plant at 30 rad/s are well above the crossover frequencies predicted by the PDT, which means that the formal QFT design will begin with nominal loop transmissions of desirable form, i.e., approximately $1/s$ in the region of crossover. Although the nominal effective plant has now changed, the PDT is not repeated as it was intended only to serve as a prelude to the formal QFT procedure.

At this juncture it is important to point out that the elements of the dynamic inverse compensator $\boldsymbol{G}_{c_p}(\boldsymbol{s})$ will involve transfer functions of order 14, i.e., the order of the effective plant. If the analyst wishes, an attempt can be made to reduce the order of these elements. This may be desirable because $\boldsymbol{G}_{c_p}(\boldsymbol{s})$ will be part of the final compensator $\boldsymbol{G}_{c_p}(\boldsymbol{s})\boldsymbol{G}_c(\boldsymbol{s})$.

Formal QFT Design

For the sake of brevity, the details of the QFT design will not be presented. The QFT technique itself has been adequately explained elsewhere, e.g., Ref. 11. The QFT design utilized the tracking performance and cross-coupling bounds created in the PDT, two of which are shown in Fig. 4. A relative stability requirement was introduced by enforcing a maximum amplitude ratio of 1.58 dB for all closed-loop tracking transfer functions. To put this number in context, for a second-order system, this amplitude peak would correspond to 5.26 dB of gain margin and 56.44 deg of phase margin. As already mentioned, allowing only small-amplitude peaking in any of the closed-loop tracking transfer functions contributes to the validity of the handling qualities and PIO evaluation where only the upper and lower tracking bounds are considered for evaluation.

The formal QFT procedure was completed using method 1, i.e., no sequential-loopclosure design was necessary.[11] After the design, closed-loop stability for each configuration was verified in a separate analysis. Figure 5 shows typical tracking and cross-coupling performance of the formal QFT design. The similarity between this figure and that for the PDT (Fig. 4) is noteworthy. The similarity in tracking performance would have been greater had the same

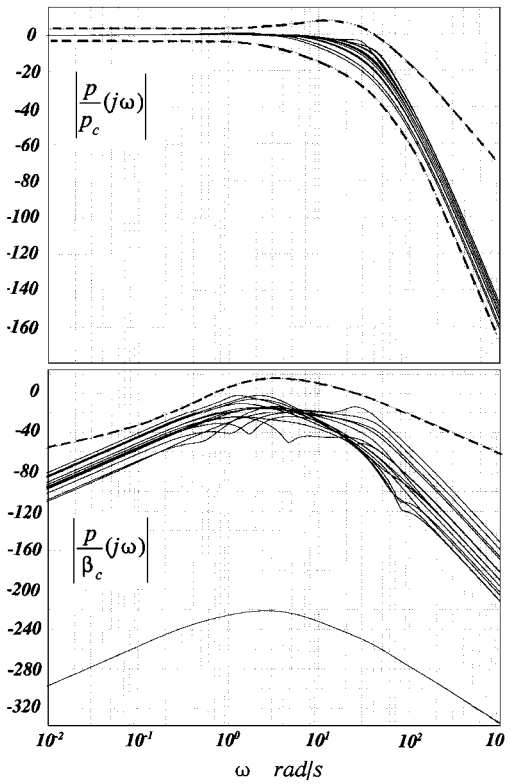

Fig. 5 Performance from formal QFT design for 15 flight conditions.

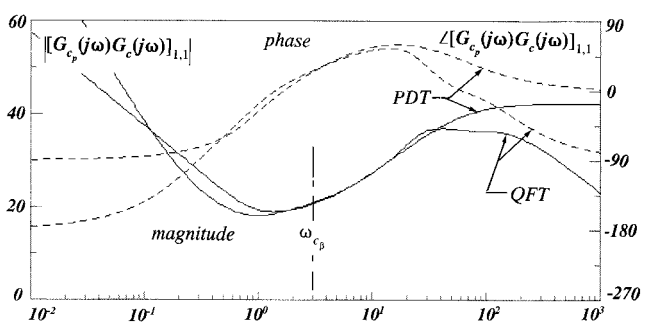

Fig. 6 Comparison of element (1, 1) of $G_{c_p}(j\omega)\cdot G_c(j\omega)$ from PDT and formal QFT designs.

prefilters been employed in the formal QFT design as in the PDT. As an example of the utility of the PDT, Fig. 6 compares the Bode diagrams for element (1, 1) in $\boldsymbol{G}_{c_p}(\boldsymbol{s})\cdot\boldsymbol{G}_c(\boldsymbol{s})$ obtained from the PDT and the formal QFT procedure. Again, the similarity is noteworthy. Finally, the crossover frequencies associated with the β and p loops for the nominal configuration were $\omega_{c_\beta} = 3.0$ and $\omega_{c_p} = 7.0$ rad/s, respectively. These compare very favorably with the results of the PDT, where values of 3.0 and 6.0 rad/s were obtained. Figure 6 also indicates that there is a significant cost of feedback associated with control of β. That is, element (1, 1) in $\boldsymbol{G}_{c_p}(\boldsymbol{s})\cdot\boldsymbol{G}_c(\boldsymbol{s})$ increases in magnitude beyond crossover and will amplify sensor noise propagated to the actuators. Similar characteristics are evident in element (1, 2), not shown. This result, which was also clearly evident in the PDT, may mean that a beta-dot sensor or estimator is warranted in this application to reduce sensor noise.

It was found that simplification of the final compensator $\boldsymbol{G}_{c_p}(\boldsymbol{s})\cdot\boldsymbol{G}_c(\boldsymbol{s})$ was possible with little impact on the magnitude or phase of $\boldsymbol{G}_{c_p}(\boldsymbol{j\omega})\cdot\boldsymbol{G}_c(\boldsymbol{j\omega})$. The elements of this final, simplified compensator are given in Table 2 along with the prefilters. Also shown are the elements of the QFT compensation matrix, alone ($\boldsymbol{G}_c(\boldsymbol{s})$). Note the simplicity of these elements. As already mentioned, the higher-order nature of the final compensator, even with some order reduction, is attributable to the dynamic inverse. Further simplification of the elements of $\boldsymbol{G}_{c_p}(\boldsymbol{s})\cdot\boldsymbol{G}_c(\boldsymbol{s})$ is possible but was not pursued. The results thus far do not consider the effects of possible

Table 2 Compensators and prefilters

Elements of $\boldsymbol{G}_{c_p}(\boldsymbol{s})\cdot\boldsymbol{G}_c(\boldsymbol{s})$

$$1,1 \rightarrow \frac{1.46\cdot 10^4[1,0.3][0.792,0.922](4.64)[0.585,19.3](20)[0.688,69.8]}{(0)^2(1)^2[0.551,22.64][1,29.9](54.8)(97.6)(101.7)}$$

$$1,2 \rightarrow \frac{77.3(0.5)(0.654)(5.23)[0.586,19.3](20)[0.693,69.7](-173)}{(0)^2(1)[0.551,22.6](30)(54.6)(95.1)[1,102]}$$

$$2,1 \rightarrow \frac{-1003(0.3)^2(3.04)(-3.34)[0.6,20](20)[0.707,30][0.59,75.0]}{(0)^2(1)[0.55,22.6][1,30][0.642,35.8](54.4)[1,99.8]}$$

$$2,2 \rightarrow \frac{183.2(0.5)(1.65)(20)[0.707,30](61.9)[0.59,75]}{(0)^2(30)[0.641,35.8](54.4)[1,98](103.4)}$$

Elements of $\boldsymbol{G}_c(\boldsymbol{s})$

$$1,1 \rightarrow \frac{1666.6(0.3)^2(20)}{(0)(1)(100)^2}, \qquad 1,2 \rightarrow 0, \qquad 2,1 \rightarrow 0$$

$$2,2 \rightarrow \frac{2.22\cdot 10^4(0.5)(20)(30)}{(0)(100)^3}$$

Prefilters

$$F_\beta = \frac{0.12(100)}{(3)(4)}, \qquad F_p = \frac{1000}{(20)(50)}$$

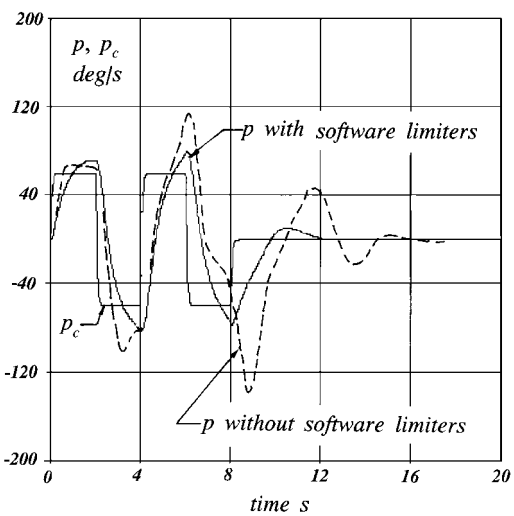

Fig. 7 Roll-rate responses to doublet roll-rate command, without and with software rate limiters.

actuator amplitude and/or rate saturation, a subject to be considered next.

Performance with Actuator Limits

Control system performance at a single flight condition was next considered, where the limitations of the actuators were introduced, i.e., performance was obtained with the actuator amplitude and rate limits given in Table 1. The flight condition was selected as Mach number of 0.3 and altitude of 10,000 ft. This condition would occur in a corner of the Mach number vs altitude plot of the 15 flight conditions. A nonlinear simulation was created that included the nonlinear actuator characteristics, with and without the software limiters of Fig. 1. No changes in the elements of the compensation matrix $\boldsymbol{G}_c(\boldsymbol{s})\cdot\boldsymbol{G}_{c_p}(\boldsymbol{s})$ were necessary other than subsuming the differentiating s into each compensator element and into $G_r(s)$ when the software limiters were used. No other changes were required because examination of $|(\beta/n_1)(j\omega)|$, $|(\beta/n_2)(j\omega)|$, $|(p/n_1)(j\omega)|$, and $|(p/n_2)(j\omega)|$ at frequencies below crossover indicated that the desired attenuation was occurring with no increases in system type.

Figure 7 shows the vehicle roll-rate response to a doublet roll-rate command consisting of four alternating pulses of 60 deg/s amplitude, each lasting 2 s. The responses without and with the software limiters are shown. The sideslip command was $\beta_c = 0$. Figures 8 and 9 show the output of the yaw thrust actuator without and with the software limiters. The figures indicate that both amplitude and rate limiting are occurring in this actuator. The performance improvement in the case when the software limiters are

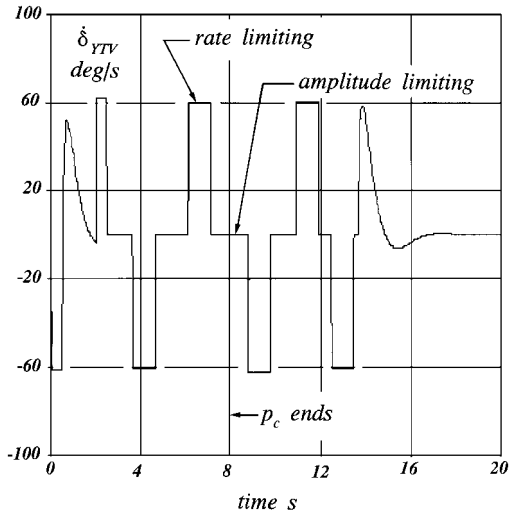

Fig. 8 Output of yaw thrust actuator without software rate limiters.

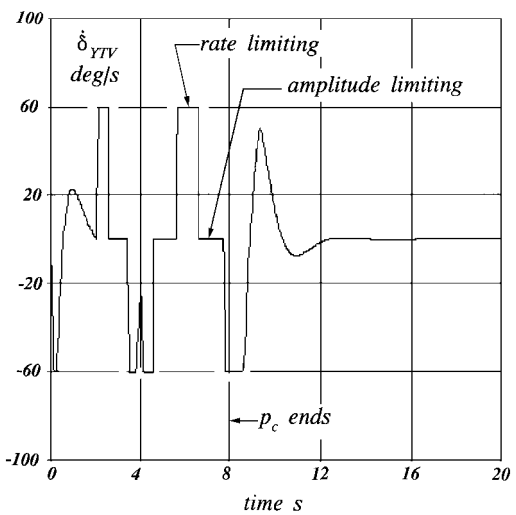

Fig. 9 Output of yaw thrust actuator with software limiters.

in operation is obvious. Note that, without the software limiters, the yaw thrust actuator remains in alternating states of rate saturation well beyond the time when the input command disappears. One important point to emphasize is that, when the software limiters are being used, the actuator in Fig. 9 is not in hard rate saturation. It is merely following a command input that takes it up to its rate limit. It is, however, occasionally experiencing amplitude saturation.

Although the software rate limiters give improved responses in many situations, the handling qualities analysis of Ref. 3 does not allow the inclusion of such nonlinearities in the analysis. Some recent progress has been made to overcome this limitation.[18,19]

Conclusions

A technique for the design of robust, decoupled flight control laws for manually controlled aircraft in which actuator rate saturation occurs has been proposed. The technique has its basis in QFT. A structural model of the human pilot is employed to provide tracking performance bounds that are predicted to yield level 1 handling qualities and no susceptibility to PIO. Dynamic inversion allows the design of a precompensation matrix that approximately decouples the flight control law and creates an effective plant that is relatively easy to compensate with the QFT procedure. A PDT allows the estimation of tracking and cross-coupling performance, cross-coupling bounds, nominal crossover frequencies, compensation elements, and prefilters prior to invoking the formal QFT design. Finally, a technique for improving control system performance in the presence of actuator rate saturation, previously limited to control structures where each actuator is driven by only one compensated error signal, is extended to control structures in which each actuator can be driven by more than one compensated error signal. A nonlinear simulation demonstrated the utility of the software limiters in improving system performance.

Acknowledgments

This research was supported by NASA Langley Research Center under Grant NAG1-1744. Barton Bacon was the Contract Technical Manager.

References

[1]Hess, R. A., and Henderson, D. K., "QFT Multi-Input, Multi-Output Design with Non-Diagonal, Non-Square Compensation Matrices," *Proceedings of the 13th World Congress: International Federation of Automatic Control* (San Francisco, CA), Vol. 8, Elsevier, Tarrytown, NY, 1996, pp. 309–314.

[2]Hess, R. A., and Snell, S. A., "Flight Control System Design with Rate Saturating Actuators," *Journal of Guidance, Control, and Dynamics*, Vol. 20, No. 1, 1997, pp. 90–96.

[3]Hess, R. A., "Unified Theory for Aircraft Handling Qualities and Adverse Aircraft-Pilot Coupling," *Journal of Guidance, Control, and Dynamics*, Vol. 20, No. 6, 1997, pp. 1141–1148.

[4]Snell, S. A., and Stout, P. W., "Robust Control of Angle of Attack Using Dynamic Inversion Combined with Quantitative Feedback Theory," AIAA Paper 96-3783, July 1996.

[5]Henderson, D. K., and Hess, R. A., "Approximations for Quantitative Feedback Theory Designs," *Journal of Guidance, Control, and Dynamics*, Vol. 20, No. 4, 1997, pp. 828–830.

[6]"Aviation Safety and Pilot Control—Understanding and Preventing Unfavorable Pilot–Vehicle Interactions," NRC Committee on the Effects of Aircraft-Pilot Coupling on Flight Safety, National Academy Press, Washington, DC, 1997.

[7]Adams, R. J., Buffington, J. M., Sparks, A. G., and Banda, S. S., "An Introduction to Multivariable Flight Control System Design," U.S. Air Force Wright Lab., WL-TR-92-3110, Wright–Patterson AFB, OH, Oct. 1992.

[8]Voulgaris, P., and Valavani, L., "High Performance Linear Quadratic and H-Infinity Designs for a Supermaneuverable Aircraft," *Journal of Guidance, Control, and Dynamics*, Vol. 14, No. 1, 1991, pp. 157–165.

[9]Osman, C., Pachter, M., and Houpis, C. H., "Active Flexible Wing Control Using QFT," *Proceedings of the 13th World Congress: International Federation of Automatic Control* (San Francisco, CA), Vol. 8, Elsevier, Tarrytown, NY, 1996, pp. 315–320.

[10]Miller, R. B., Horowitz, I. M., Houpis, C. H., and Barfield, A. F., "Multi-Input, Multi-Output Flight Control System Design for the YF-16 Using Nonlinear QFT and Pilot Compensation," *International Journal of Robust and Nonlinear Control*, Vol. 4, No. 1, 1994, pp. 211–230.

[11]Houpis, C. H., "Quantitative Feedback Theory (QFT) for the Engineer, A Paradigm for the Design of Control Systems for Uncertain Nonlinear Plants," Flight Dynamics Directorate, U.S. Air Force Wright Lab., WL-TR-95-3061, Wright–Patterson AFB, OH, June 1995.

[12]Horowitz, I., "Survey of Quantitative Feedback Theory," *International Journal of Control*, Vol. 53, No. 2, 1991, pp. 255–291.

[13]Catapang, D. R., Tischler, M. B., and Biezad, D. J., "Robust Crossfeed Design for Hovering Rotorcraft," *International Journal of Robust and Nonlinear Control*, Vol. 4, No. 1, 1994, pp. 161–180.

[14]Yaniv, O., "MIMO QFT Using Non-Diagonal Controllers," *International Journal of Control*, Vol. 61, No. 1, 1995, pp. 245–253.

[15]Enns, D., Bugajski, D., Hendrick, R., and Stein, G., "Dynamic Inversion: An Evolving Methodology for Flight Control," *International Journal of Control*, Vol. 59, No. 1, 1994, pp. 71–91.

[16]Snell, S. A., "Decoupling Control Law Design with Applications to Flight," AIAA Paper 98-0500, Jan. 1998.

[17]Klyde, D. H., McRuer, D. T., and Myers, T. T., "Pilot-Induced Oscillation Analysis and Prediction with Actuator Rate Limiting," *Journal of Guidance, Control, and Dynamics*, Vol. 20, No. 1, 1997, pp. 81–89.

[18]Hess, R. A., and Stout, P. W., "Assessing Aircraft Susceptibility to Nonlinear Aircraft-Pilot Coupling/Pilot-Induced Oscillations," AIAA Paper 97-3496, Aug. 1997.

[19]Hess, R. A., "Predicting Handling Qualities Levels for Vehicles with Nonlinear Dynamics," AIAA Paper 98-0494, Jan. 1998.